Table S1. Summary of selected satellite sensors.

Sensor mission	Organization	Operation period	Band	Spatial resolution (m)	Swath (km)	Spectral coverage (um)	Number of channels	Ref.
Landsat Oli-8	NASA and USGS collaboration	2013	1 2 ;3 ;4 5 6 7 8 9 10 11	30 (Coastal aerosol) 30 (Visible) 30 (NIR) 30 (SWIR-1) 30 (SWIR-2) 15 (Panchromatic) (Cirrus) 100 (TIR-1) 100 (TIR-2)	185	0.43 – 0.45 0.45 – 0.67 0.85 – 0.88 1.57 – 1.65 2.11 – 2.29 0.50 - 0.68 1.36 - 1.38 10.60 – 11.19 11.50 – 12.51	11	[1,2]
ASTER (EOS Terra	NASA and MITI USA	1999		15 (VNIR) 30 (SWIR) 90 (TIR)	60	0.52 – 0.86, 1.60 – 2.43, 8.125–11.65	14	[3,4]

Table S2. Details of the most color composite used in geology.

Colore Composite (R-G-B)	Interest	Imagery	Reference
4-3-2	natural colour	Landsat 8	[5]
2-5-7 and 6-5-7	iron oxides and clay minerals	Landsat 8	[6]
10-11-7	silicate detection	Landsat 8	[6]
5-7-3	Hydrothermally altered rocks	Landsat 8	[7]
7-6-4 and 5-6-7	Rock discrimination of alteration	Landsat 8	[8]
3-2-7 2-3-11 7-3-11	Li-bearing minerals	Landsat 8	[7]
6-2-1	gossan areas, alteration zones and host rocks	ASTER	[7]
6-3-1	Enhance hydrothermal gossans	ASTER	[7]
7-4-2	identify and enhance geological structures	ASTER	[7]

Table S3. Details band ratios usefulness in geological studies.

Ratio and Band Ratio (R-G-B)	Useful	Imagery	reference
4/2 or 4/3	Iron oxides	Landsat 8	[7]
7/6	clay minerals mapping (kaolinite, illite and montmorillonite)	Landsat 8	[8]
7/6	Muscovite	ASTER	[7]
3/5 2/4	discriminate Li-mineralizations	Landsat 8 ASTER	[7]
6⁄5 5/3	sandstone–mudstone mapping	Landsat 8 ASTER	[4]
5⁄4 3⁄2	discriminate alluvium	Landsat 8 ASTER	[4]
4⁄7 3⁄6	Rock unit mapping	Landsat 8 ASTER	[4]
9⁄4	Discrimination rhyolitic ignimbrite	ASTER	[4]
4/2 - 6/7 - 5	Identification of lithology and altered rocks	Landsat 8	[8]
4/2 - 6/7 - band 10	lithological mapping	Landsat 8	[6]
4/2 - 6/5 - band 6/7	hydrothermal alteration area mapping	Landsat 8	[6]
6/7 - 6/5 - 4/2	clay and carbonate minerals mapping	Landsat 8	[9]

Table S4. Accuracy assessment for SAM for SAM classification of ASTER image.

	Quaternary basalt	Trachy-Andesite	Water	Vegetation	Miocene	Jurassic	Old quaternary	Recent Quaternary	Eociene and oligocene	User Accuarcy
Quaternary basalt	298	2	1	23	2	0	1	0	0	91.13
Trachy-Andesite	1	267	13	8	2	1	3	8	2	87.54
Water	0	35	345	3	19	2	0	0	8	83.73
Vegetation	8	0	2	192	0	0	2	2	4	93.2
Miocene	1	6	0	0	78	7	5	4	2	75.72
Jurassic	2	0	0	0	1	62	2	3	9	78.48
Old quaternary	5	0	0	0	0	0	58	6	11	72.5
Recent Quaternary	6	1	2	7	6	3	7	205	9	83.33
Eociene and oligocene	2	7	0	3	5	18	13	26	94	55.95
Producer Accuarcy	92.26	83.96	95.04	81.355	69.02	66.66	63.73	80.70	67.62	OA=0.83

Table S4. Accuracy assessment for SAM for SAM classification of Landsat 8-OLI image.

	Quaternary basalt	Trachy-Andesite	Water	Vegetation	Miocene	Jurassic	Old quaternary	Recent Quaternary	Eociene and oligocene	User Accuarcy
Quaternary basalt	121	8	3	14	0	7	5	31	3	63.02
Trachy-Andesite	1	237	17	4	0	9	0	30	5	78.21
Water	3	25	119	3	9	2	10	0	8	66.48
Vegetation	11	0	2	142	0	0	11	12	14	79.77
Miocene	1	0	0	0	89	3	16	8	0	76.06
Jurassic	0	0	21	4	3	123	8	2	16	69.491
Old quaternary	7	0	0	0	0	10	76	0	41	56.71
Recent Quaternary	9	1	2	2	9	10	0	185	9	59.03
Eociene and oligocene	2	8	0	13	5	11	9	5	134	71.65
Producer Accuarcy	78.064	84.94	72.56	78.021	77.39	70.28	56.29	67.76	58.26	OA=0.72

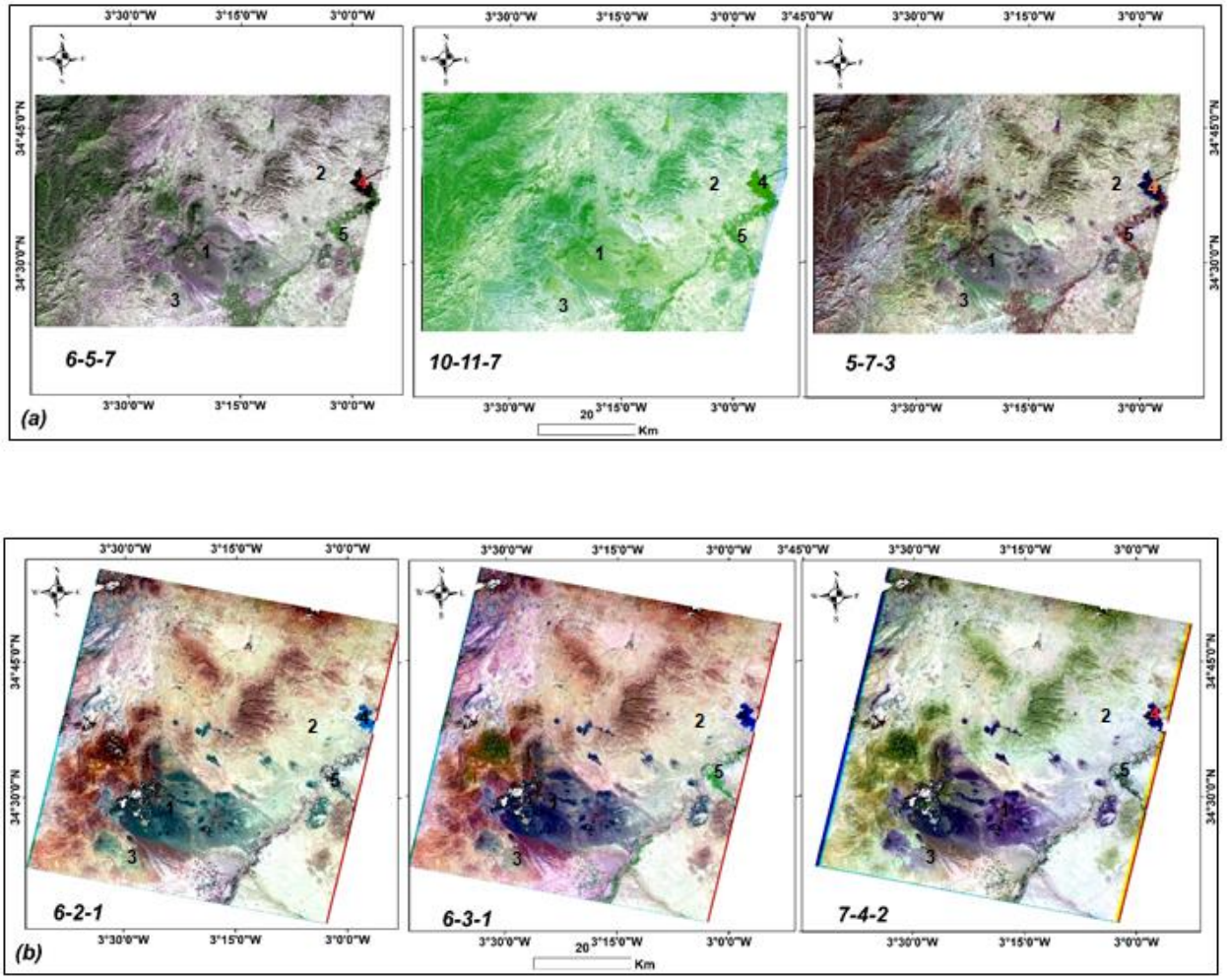

Figure S1. False color composite (a. Landsat oli-8 and b. ASTER).

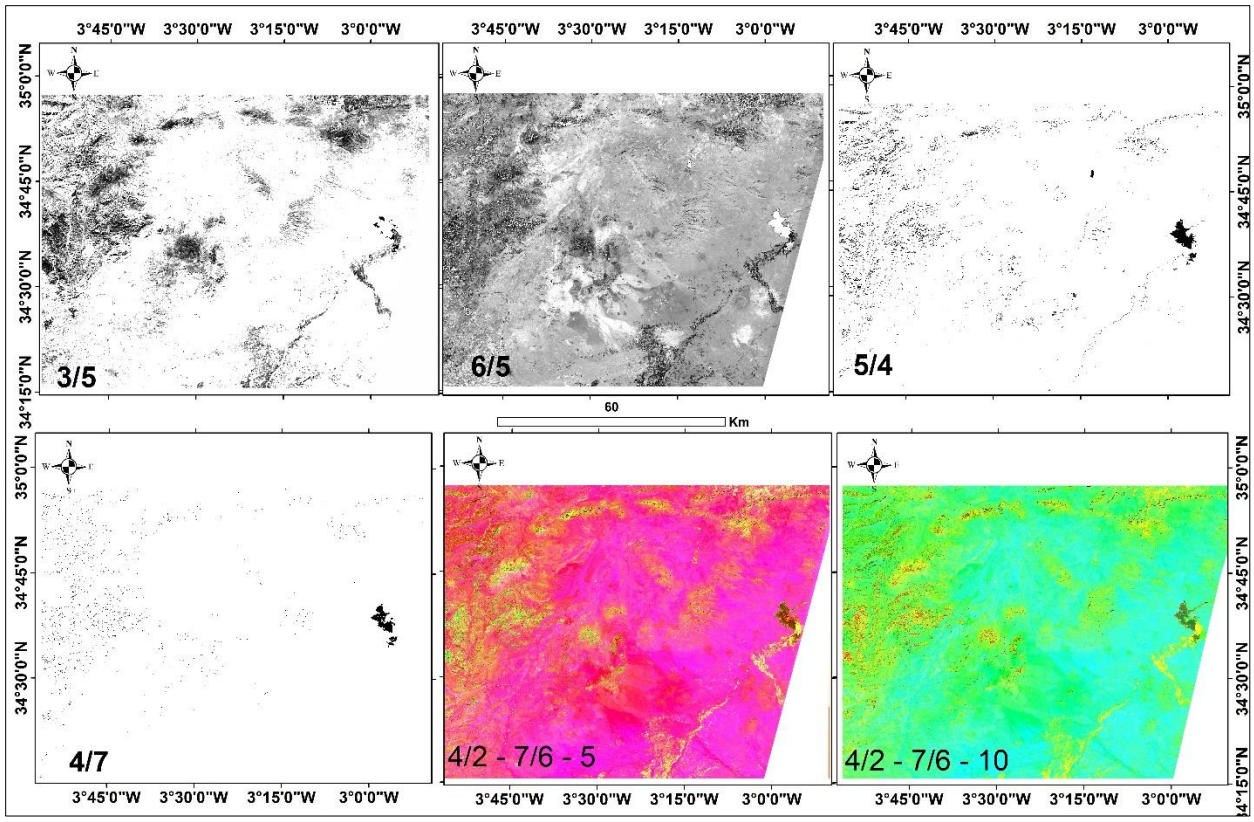

Figure S2. Landsat 8 Oli bands ration used in geology.

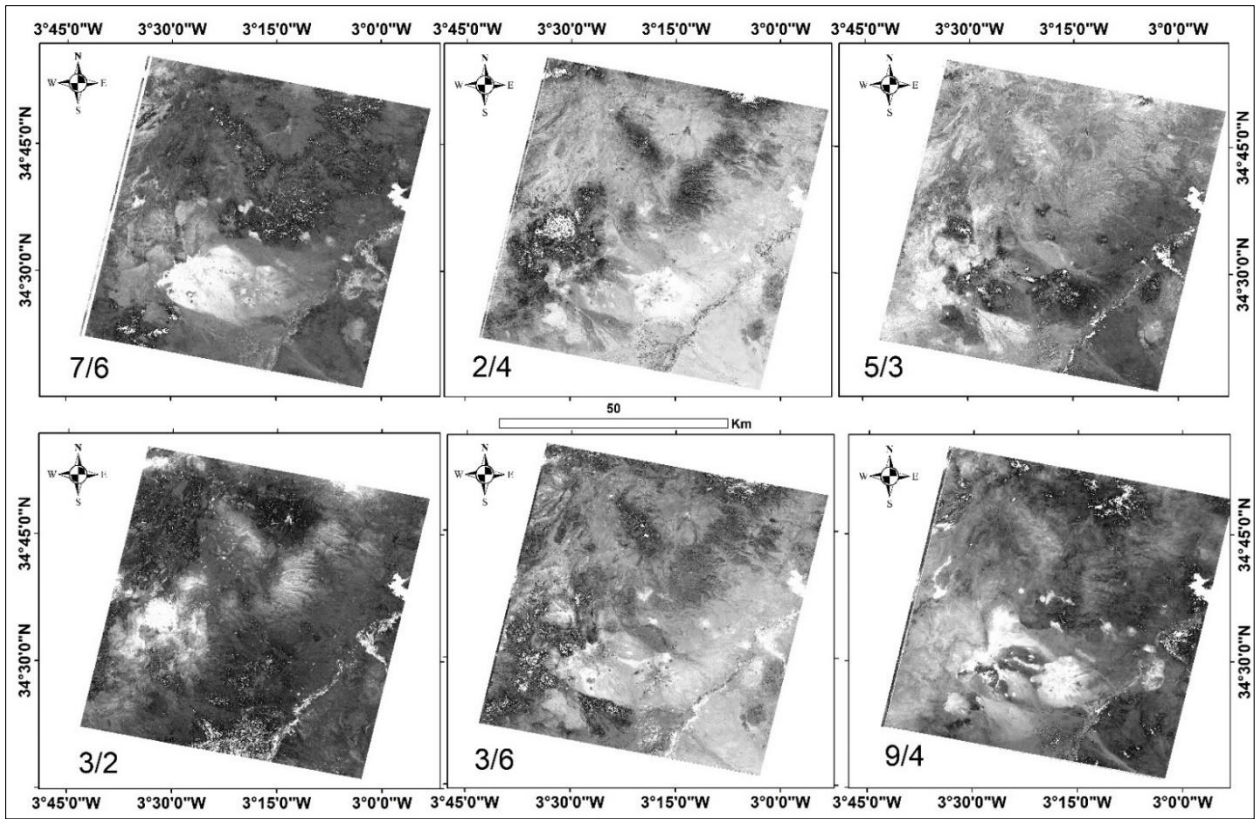

Figure S3. ASTER bands ration used in geology.

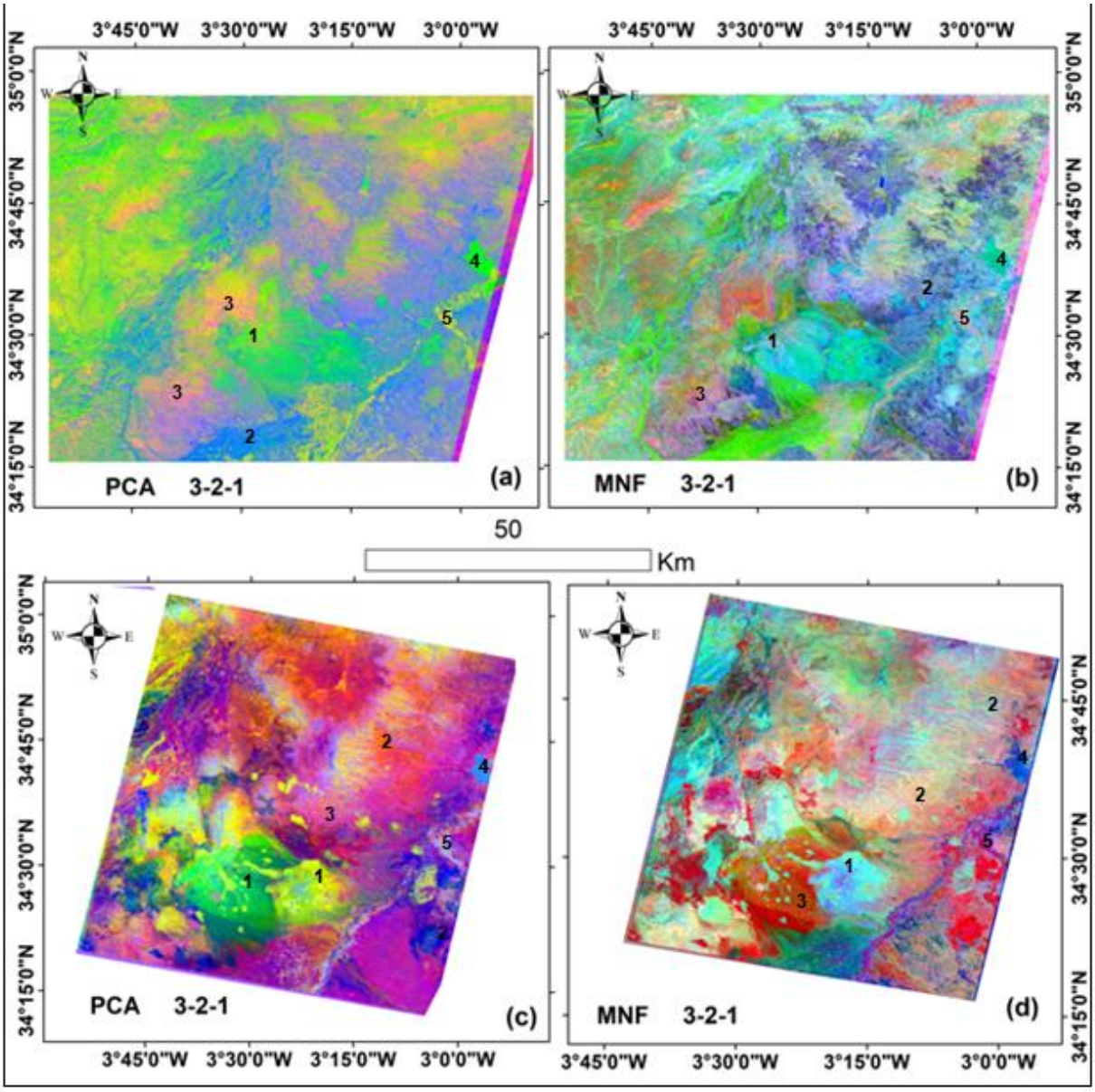

Figure S4. PCA Composite bands 3, 2, 1 (a. Landsat 8 Oli and c. ASTER) and MNF Composite bands 3, 2, 1 (b. Landsat 8 Oli and d. ASTER).

References

1. Korhonen, L.; Packalen, P.; Rautiainen, M. Comparison of Sentinel-2 and Landsat 8 in the Estimation of Boreal Forest Canopy Cover and Leaf Area Index. *Remote Sens. Environ.* **2017**, *195*, 259–274.
2. Roy, D.P.; Wulder, M.A.; Loveland, T.R.; Woodcock, C.E.; Allen, R.G.; Anderson, M.C.; Helder, D.; Irons, J.R.; Johnson, D.M.; Kennedy, R. Landsat-8: Science and Product Vision for Terrestrial Global Change Research. *Remote Sens. Environ.* **2014**, *145*, 154–172.
3. Rogan, J.; Chen, D. Remote Sensing Technology for Mapping and Monitoring Land-Cover and Land-Use Change. *Prog. Plan.* **2004**, *61*, 301–325.

4. Adiri, Z.; El Harti, A.; Jellouli, A.; Maacha, L.; Bachaoui, E.M. Lithological Mapping Using Landsat 8 OLI and Terra ASTER Multispectral Data in the Bas Drâa Inlier, Moroccan Anti Atlas. *J. Appl. Remote Sens.* **2016**, *10*, 016005.
5. Abdulmalik, N.; Garba, I.; Abubakar, I.Y.; Muhyideen, H.; Agunleti, Y.S.; Magaji, S.S.; Aliyu, A.E.; Umaru, A.O. APPLICATION OF LANDSAT-8 OPERATIONAL LAND IMAGER AND SHUTTLE RADAR TOPOGRAPHY MISSION-DIGITAL ELEVATION MODEL IN THE STUDY OF IKARA AND ITS ENVIRONS, NORTHWESTERN NIGERIA. *FUDMA J. Sci.* **2021**, *5*, 259–273.
6. Ali, A.S.; Pour, A.B. Lithological Mapping and Hydrothermal Alteration Using Landsat 8 Data: A Case Study in Ariab Mining District, Red Sea Hills, Sudan. *Int. J. Basic Appl. Sci.* **2014**, *3*, 199.
7. Cardoso-Fernandes, J.; Teodoro, A.C.; Lima, A. Remote Sensing Data in Lithium (Li) Exploration: A New Approach for the Detection of Li-Bearing Pegmatites. *Int. J. Appl. Earth Obs. Geoinformation* **2019**, *76*, 10–25.
8. Banerjee, K.; Jain, M.K.; Panda, S.; Jeyaseelan, A.T. Landsat 8 OLI Data for Identification of Hydrothermal Alteration Zone in Singhbhum Shear Zone Using Successive Band Depth Difference Technique-a New Image Processing Approach. *Curr. Sci. 00113891* **2019**, *116*.
9. Traore, M.; Wambo, J.D.T.; Ndepete, C.P.; Tekin, S.; Pour, A.B.; Muslim, A.M. Lithological and Alteration Mineral Mapping for Alluvial Gold Exploration in the South East of Birao Area, Central African Republic Using Landsat-8 Operational Land Imager (OLI) Data. *J. Afr. Earth Sci.* **2020**, *170*, 103933.